Available online at www.sciencedirect.com
ScienceDirect
Journal of Power Sources 176 (2008) 353–358
JOURNAL OF POWER SOURCES
www.elsevier.com/locate/jpowsour

Short communication

Spherical silicon/graphite/carbon composites as anode material for lithium-ion batteries

Jong-Hyuk Lee, Wan-Jun Kim, Jae-Youn Kim, Sung-Hwan Lim, Sung-Man Lee *

Department of Advanced Materials Science and Engineering, Kangwon National University, Chuncheon, Kangwon-Do 200-701, Republic of Korea

Received 28 June 2007; received in revised form 22 September 2007; accepted 28 September 2007
Available online 18 October 2007

Abstract

A spherical nanostructured Si/graphite/carbon composite is synthesized by pelletizing a mixture of nano-Si/graphite/petroleum pitch powders, followed by heat treatment at 1000 °C under an argon atmosphere. The structure of the composite sphere is examined by transmission electron microscopy (TEM) and scanning electron microscopy (SEM) with energy dispersive X-ray analysis (EDAX). The resultant composite sphere consists of nanosized silicon and flaked graphite embedded in a carbon matrix pyrolyzed from petroleum pitch, in which the flaked graphite sheets are concentrically distributed in a parallel orientation. The composite material exhibits good electrochemical properties, a high reversible specific capacity of ~700 mAh g^{-1}, a high coulombic efficiency of 86% on the first cycle, and a stable capacity retention. The enhanced electrochemical performance is attributed to the structural stability of the composite sphere during the charging–discharging process.

Keywords: Silicon/graphite/carbon composite; Anode material; Lithium-ion battery; Spherical composite; Electrochemical performance; Specific capacity

1. Introduction

Lithium-ion batteries containing graphite anodes are now the most widely used power sources for portable electronic devices. For commercial applications, however, lithium-ion batteries with high specific energy density are in increasing demand. Recently, various anode materials have been proposed to overcome the limited capacity of graphite (372 mAh g^{-1}). Much attention has been given to silicon-based anode materials because silicon has the high specific capacity of 4200 mAh g^{-1}. Unfortunately, silicon undergoes a change in volume change during lithium-ion insertion and extraction, and this result in mechanical instability and poor cycleability [1,2]. Therefore, in order to obtain better cycleability for silicon-based anodes, the mechanical stresses induced by the large volumetric change should be buffered. Many attempts to solve this problem have been made [3–28]. For example, silicon–graphite–carbon composite systems in which ultra fine silicon particles are dispersed uniformly in a ductile matrix of graphite and the mixtures are coated with carbon, are quite promising for practical applications [22–28]. The electrochemical performance of such composites appears to be dependent on the preparation method and the resultant structure of the composite. Moreover, it is well known that spherically shaped anode material is preferable as a means of improving the anode characteristics due to its high tapping density [29,30].

In this study, a spherical silicon–graphite–carbon composite anode material for lithium-ion batteries, is prepared and found to exhibit a large charge–discharge capacity and excellent cycle performance.

2. Experimental

Spherical nano-Si/graphite/carbon composite powders were fabricated as follows. Nano-Si (99.9%, 100 nm, Nanostructured

* Corresponding author. Tel.: +82 33 250 6266; fax: +82 33 242 6256.
E-mail address: smlee@kangwon.ac.kr (S.-M. Lee).

0378-7753/$ – see front matter © 2007 Elsevier B.V. All rights reserved.
doi:10.1016/j.jpowsour.2007.09.119

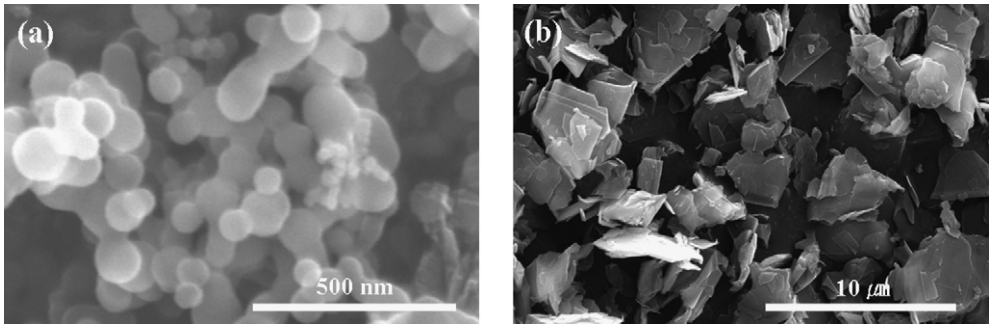

Fig. 1. SEM images of (a) nano-silicon and (b) natural flake graphite.

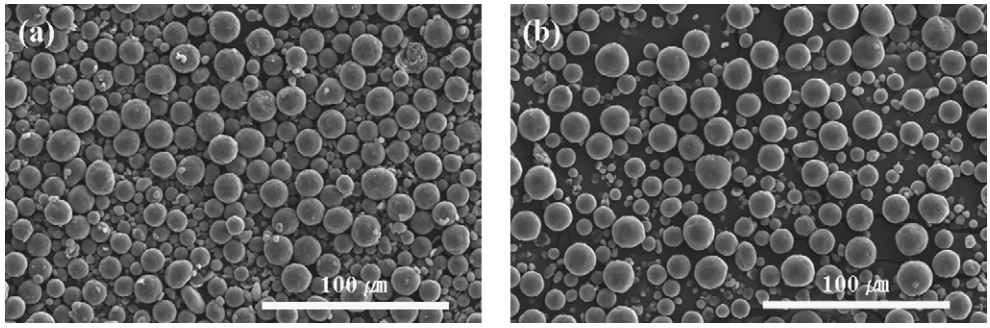

Fig. 2. SEM images of (a) the composite precursor and (b) composite particles.

& Amorphous Materials Inc.) and natural graphite (~5 μm) powders were mixed in a weight ratio of 30:70. The elemental powders were mixed with a tetrahydrofuran solution in which a pitch (carbon yield, 76%, provided by Carbonix Inc., South Korea) as a carbon precursor was dissolved in 33 wt.% of the mixture, agitated using a ball milling method, and finally vacuum-dried at 100 °C for 6 h. The dried composite was inserted into an agglomerator to prepare the first spherical composite particles. Then, the first composite particles and petroleum-based pitch powders were mixed in a weight ratio of 87:13, followed by pelletizing and heating under an argon atmosphere at 1000 °C. The pelletizing process was performed in an air atmosphere. The particle morphology and electrode cross-section were examined by SEM with EDAX equipment. A TEM analysis was performed to observe the structure and dispersion of the components in the nano-Si/graphite/carbon composite particles. The sample for TEM analysis was prepared by means of a focused ion beam (FIB) technique. The phase components of the composite material were investigated by powder X-ray diffractometry (XRD) with Cu Kα radiation.

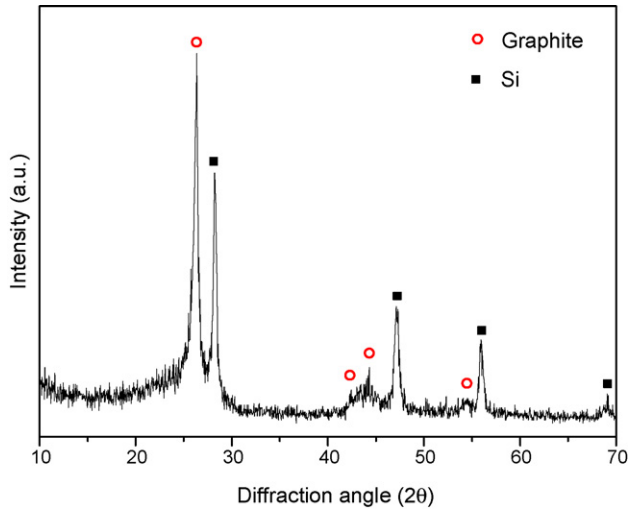

Fig. 3. XRD pattern of the composite material.

The electrodes were prepared by pasting an aqueous slurry containing 90 wt.% composite powder, 5 wt.% carbon black, 3.3 wt.% styrene butadiene rubber (SBR) as a binder, and 1.7 wt.% carboxymethyl cellulose (CMC) as a surface-active agent, on to a copper foil of 10 μm thickness. The electrodes were then dried at 120 °C for 12 h under vacuum and subsequently pressed. The electrolyte was 1 M $LiPF_6$ in a mixture of ethylene carbonate (EC) and diethyl carbonate (DEC) (1:1, v/v, provided by Cheil Industries Inc., South Korea). 2016 coin-type half-cells were fabricated using a metallic lithium foil as a counter electrode.

The cycling performance of the cells was evaluated in a constant current–constant–voltage (CC–CV) mode for the initial two cycles and thereafter in constant–current (CC) mode. The CC–CV test was performed by holding the current at 0.2 mA cm^{-2} until the potential dropped to 0.02 V and then maintaining this potential until the current decreased to 0.1 mA cm^{-2}. For the CC test, the charge–discharge current was 0.2 mA cm^{-2} and the cut-off voltage was set between 0.02 and 1.5 V.

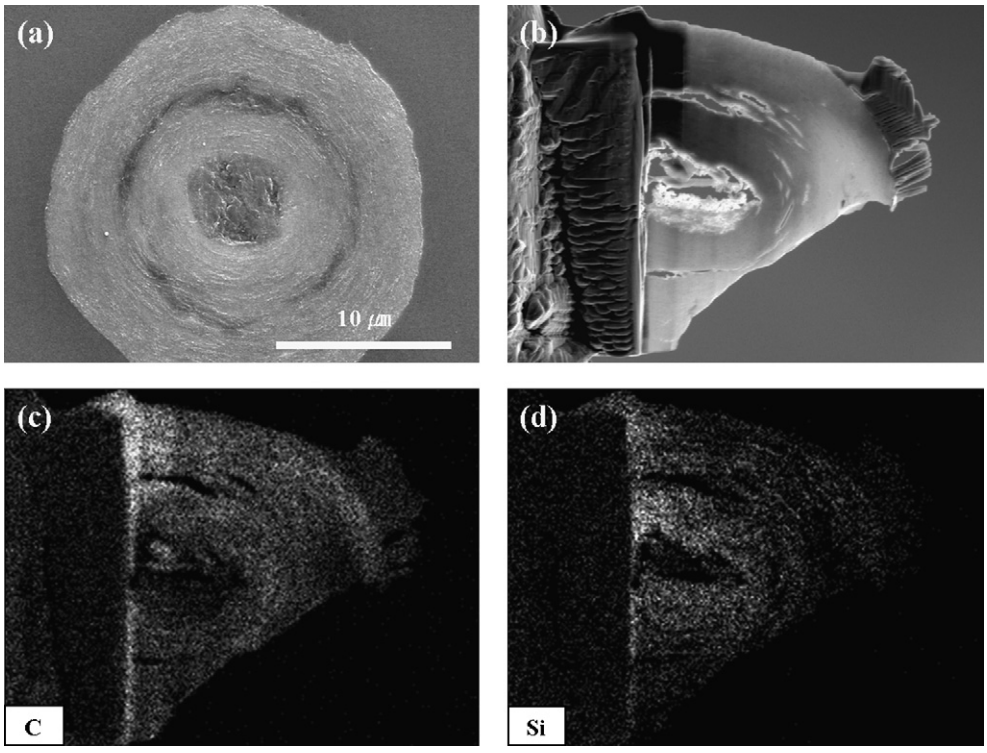

Fig. 4. Cross-section SEM images of silicon/graphite/carbon composite sphere (a and b) and EDAX maps of (c) silicon and (d) carbon. Note that the sample for (b) is obtained using a FIB workstation.

3. Results and discussion

The SEM images of the nano-silicon and natural flake graphite, used to prepare the Si/graphite/carbon composite materials, are shown in Fig. 1. The Si powders show an uniform particle-size distribution between 50 and 100 nm. The overall particle shape of graphite was thin and flat, and the median diameter was 5 μm.

The composite material was prepared by pelletizing a mixture of nano-silicon/graphite/petroleum pitch in a weight ratio of 20:47:33, using a method which is similar to that for making spheres from flaky graphite [31], followed by a second pelletizing of the first pelletized powders and petroleum pitch powders in a weight ratio of 87:13. The resultant composite precursor was heat-treated at 1000 °C for 1 h in an argon atmosphere to obtain the nano-silicon/graphite/carbon composite. Fig. 2 shows the SEM images of the composite precursor and composite particles. It is seen that spherical particles of the composite precursor are obtained, and that this shape is maintained after heat treatment at 1000 °C. The XRD pattern of the composite material is shown in Fig. 3. There exists only the crystalline diffraction peaks of the silicon and graphite in addition to a broadened diffused peak at around $2\theta = 26^\circ$ that is attributable to the disordered pitch carbon. Notably, no other impurity phases, such as SiC, are detected.

In order to examine the microstructure of the composite particles, SEM and TEM analyses were conducted. Typical cross-section SEM images of the Si/graphite/carbon composite spheres are presented in Fig. 4a and b. It should be noted that the image in Fig. 4b was obtained using a FIB workstation, and in the

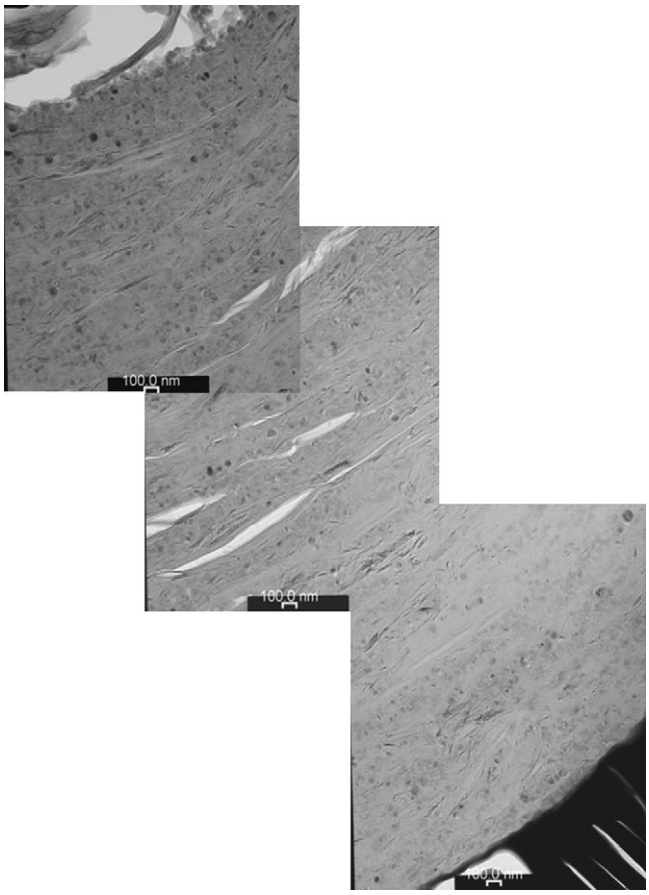

Fig. 5. Cross-sectional TEM images of silicon/graphite/carbon composite sphere.

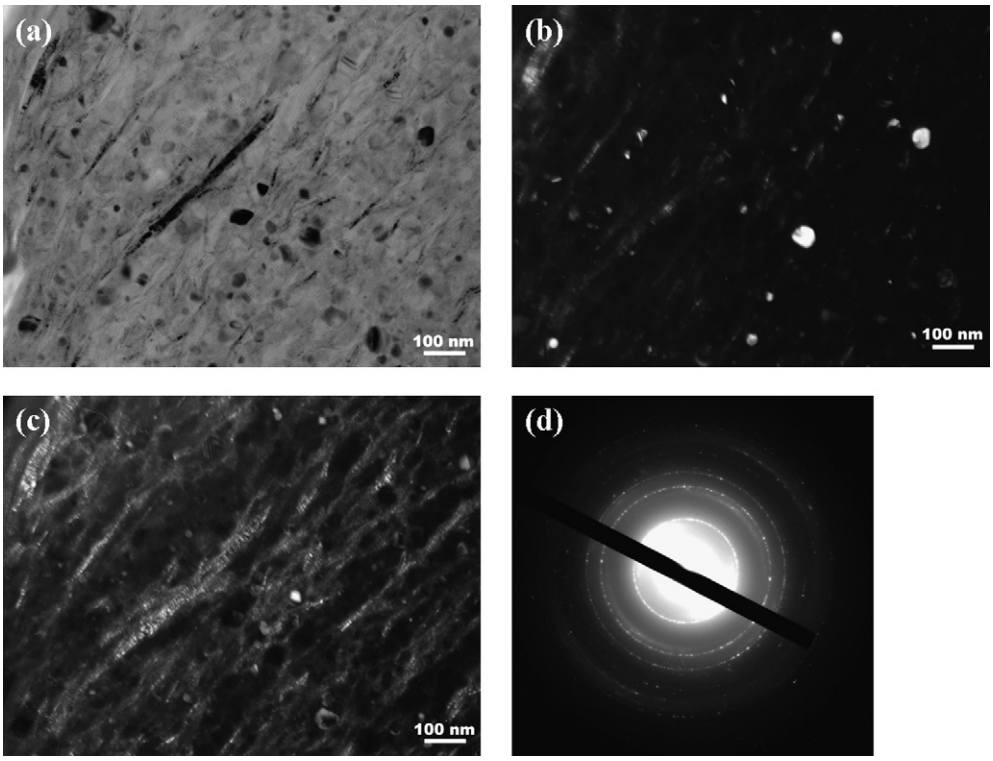

Fig. 6. High-magnification TEM micrographs of silicon/graphite/carbon composite: (a) bright-field, (b) dark-field (Si), (c) dark-field (graphite) and (d) selected area diffraction pattern.

process, part of the sample was broken. A microscale hole and cracks inside the composite sphere are found. The EDAX elemental mapping images shown in Fig. 4c and d indicate that the silicon content is higher in the centre region than in the surface region, which originates from the composite sphere making process, that is conducted in sequential steps as described in Section 2. The composite particles consist of concentric flaked graphite in a parallel orientation, which combined to form spherical particles as shown in Fig. 5. Magnified cross-sectional TEM images

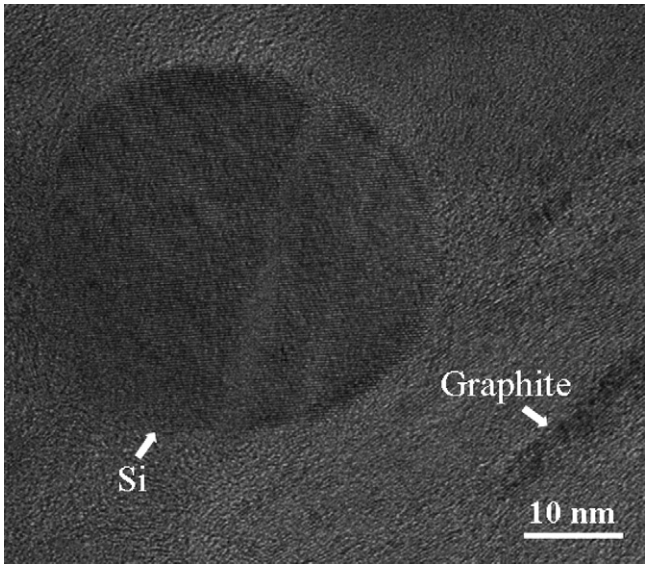

Fig. 7. High-resolution TEM image of composite.

are given in Fig. 6. The bright- and dark-field images reveal that Si nanocrystallites and thin graphite sheets of nanosize thickness are finely distributed in the carbon matrix pyrolyzed from the petroleum pitch. The selected area diffraction pattern (SADP) exhibits well-defined rings with spots that can be indexed to crystalline Si as well as diffused rings corresponding to nanosize graphite, There is no indication of the presence of SiC. It is also found that the flaked graphite sheets are very thin (50–100 nm). A high-resolution image of the composite is given in Fig. 7. Lattice fringes corresponding to the nanocrystalline Si and nanosize graphitic stacks are visible. The nanocrystalline Si is surrounded with amorphous carbon but without forming any compound such as SiC.

Fig. 8 shows the charge (Li insertion)–discharge (Li extraction) curves of the Si/graphite/carbon composite for the first and second cycles, charged in CC–CV mode and discharged in CC mode. The reversible capacity obtained by the CC mode is ~700 mAh g^{-1} which is maintained during cycling up to 50 cycles. The reversible capacity and the coulombic efficiency of the composite electrode as a function of cycle number are presented in Fig. 9. The composite exhibits very stable capacity retention behavior and high coulombic efficiency, with a first-cycle efficiency of 86 and >99% efficiency for the subsequent cycles. The morphological changes of the composite electrode before and after 50 cycles were examined by SEM (Fig. 10). They reveal a similar surface morphology. Notably, after 50 cycles, no cracks are formed. These results indicate that the microstructure of the nano-Si/graphite/carbon composite sphere is very effective in buffering the volume expansion of Si during

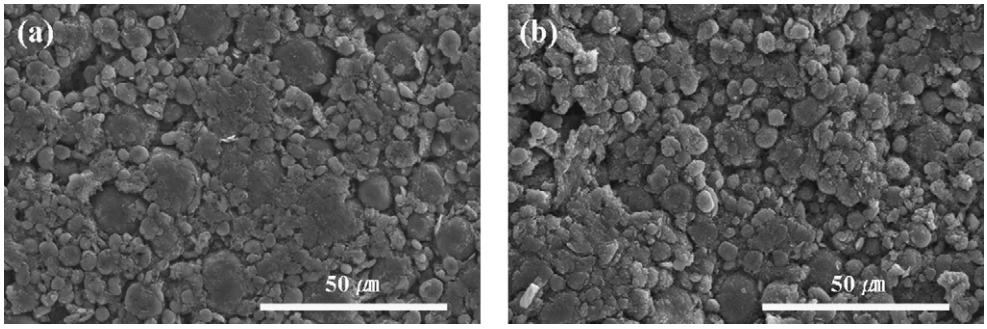

Fig. 10. Morphology of composite electrode: (a) before cycling and (b) after 50 cycles.

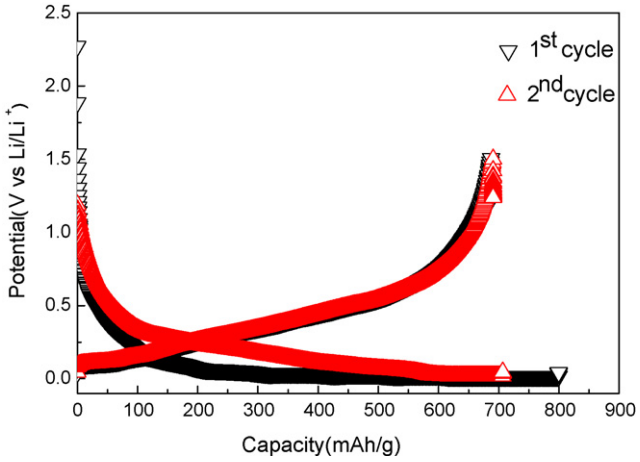

Fig. 8. Charge–discharge curves of Si/graphite/carbon composite for first and second cycles.

cycling. Moreover, since spherical particles lead to an improved tap density, the resultant spherically shaped composites are highly desirable as anode materials for lithium-ion batteries. It is also worthwhile to the note that the present composite sphere is fabricated by a simple process, which is similar to that used to obtain spheroidal shapes from flaky natural graphites [31]. Higher capacity of the nano-si/graphite/carbon composite can be achieved by increasing the Si content, but if the Si content is increased, the fabrication conditions including the weight ratio of the composite components and the size of the composite particles, need to be optimized in order to obtain an enhanced cycle performance. Relevant studies are currently in progress, and the results will be reported in subsequent publications.

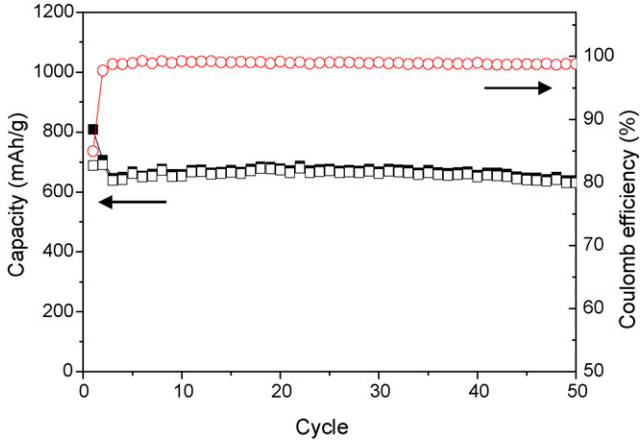

Fig. 9. Charge–discharge capacities and coulombic efficiency of composite electrode as function of cycle number.

4. Conclusions

A nano-Si/graphite/carbon composite of spherical shape is synthesized by pelletizing a mixture of nano-Si/graphite/petroleum pitch powders, followed by pyrolysis at 1000 °C under an argon atmosphere. The composite sphere, as indicated by SEM–EDAX and TEM analyses, consisted of nanosized silicon and flaked graphite embedded in a carbon matrix pyrolyzed from petroleum pitch, in which the thin graphite sheets are concentrically distributed in a parallel orientation. The composite shows a high reversible capacity of ~700 mAh g^{-1}, along with an initial coulombic efficiency of 86 % and good cycleability. The good electrochemical performance is attributed to the enhanced structural stability of the composite sphere, in which the stress induced by the volume change of the silicon phase during cycling is effectively buffered.

Acknowledgement

This work was supported by the Ministry of Information & Communications, Korea, under the Information Technology Research Center (ITRC) Support Program.

References

[1] T.D. Besenhard, J. Yang, M. Winter, J. Power Sources 68 (1997) 87–90.
[2] C.J. Wen, R.A. Huggins, J. Solid State Chem. 37 (1976) 271–278.
[3] A.M. Wilson, J.R. Dahn, J. Electrochem. Soc. 142 (1995) 326–332.
[4] H. Li, X. Huang, L. Chen, Z. Wu, Y. Liang, Electrochem. Solid State Lett. 2 (1999) 547–549.
[5] I.-S. Kim, P.N. Kumta, G.E. Blomgren, Electrochem. Solid State Lett. 3 (2000) 493–496.
[6] I.-S. Kim, G.E. Blomgren, P.N. Kumta, J. Power Sources 130 (2004) 275–280.
[7] M. Yoshio, H. Wang, K. Fukuda, T. Umeno, N. Dimov, Z. Ogumi, J. Electrochem. Soc. 149 (2002) A1598–A1603.
[8] N. Dimov, S. Kugino, M. Yoshio, Electrochim. Acta 48 (2003) 1579–1587.
[9] J. Yang, B.F. Wang, K. Wang, Y. Liu, J.Y. Xie, Z.S. Wen, Electrochem. Solid State Lett. 6 (2003) A154–A156.
[10] H. Dong, X.P. Ai, H.X. Yang, Electrochem. Commun. 5 (2003) 952–957.
[11] H.Y. Lee, S.M. Lee, J. Power Sources 112 (2002) 649–654.

[12] Y. Liu, K. Hanai, T. Matsumura, N. Imanishi, A. Hirano, Y. Takeda, Electrochem. Solid State Lett. 7 (2004) A492–A495.
[13] M.S. Park, Y.J. Lee, S. Rajendran, M.S. Song, H.S. Kim, J.Y. Lee, Electochim. Acta 50 (2005) 5561–5567.
[14] H.Y. Lee, Y.L. Kim, M.K. Hong, S.M. Lee, J. Power Sources 141 (2005) 159–162.
[15] J. Yang, Y. Takeda, N. Imanishi, C. Capiglia, J.Y. Xie, O. Yamamoto, Solid State Ionics 152/153 (2002) 125–129.
[16] X. Yang, J. McBreen, W. Yoon, M. Yoshio, H. Wang, K. Fukuda, T. Umeno, Electrochem. Commun. 4 (2002) 893–897.
[17] N. Dimov, S. Kugino, M. Yoshio, J. Power Sources 136 (2004) 108–114.
[18] G.X. Wang, J. Yao, H.K. Liu, Electrochem. Solid State Lett. 7 (2004) A250–A253.
[19] T. Kim, S. Park, S.M. Oh, Electrochem. Commun. 8 (2006) 1461–1467.
[20] J.H. Kim, H. Kim, H.J. Sohn, Electrochem. Commun. 7 (2005) 557–561.
[21] B.C. Kim, H. Uono, T. Sato, T. Fuse, T. Ishihara, M. Senna, Solid State Ionics 172 (2004) 33–37.
[22] T. Morita, N. Takami, J. Electrochem. Soc. 153 (2006) A425–A430.
[23] B.C. Kim, H. Uono, T. Satou, T. Fuse, T. Ishihara, M. Ue, M. Senna, J. Electrochem. Soc. 152 (2005) A523–A526.
[24] H.Y. Lee, S.M. Lee, Electrochem. Commun. 6 (2004) 465–469.
[25] Y. Zhang, X.G. Zhang, H.L. Zhang, Z.G. Zhao, F. Li, C. Liu, H.M. Cheng, Electrochim. Acta 51 (2006) 4994–5000.
[26] M.K. Datta, P.N. Kumta, J. Power Sources 158 (2006) 557–563.
[27] M. Holzaptel, H. Buqa, F. Krumeich, P. Novak, F.-M. Petrat, C. Veit, Electrochem. Solid State Lett. 8 (2005) A516–A520.
[28] H. Uono, B.C. Kim, T. Fuse, M. Ue, J. Yamaki, J. Electrochem. Soc. 153 (2006) A1708–A1713.
[29] Y. Chen, G.X. Wang, J.P. Tian, K. Konstantinov, H.K. Liu, Electrochim. Acta 50 (2004) 435–441.
[30] M. Yoshio, H. Wang, Y.S. Lee, K. Fukuda, Electrochim. Acta 48 (2003) 791–797.
[31] M. Yoshio, H.Y. Wang, K. Fukuda, Angew. Chem. Int. Ed. 42 (2003) 4203–4206.